Supplementary Figures

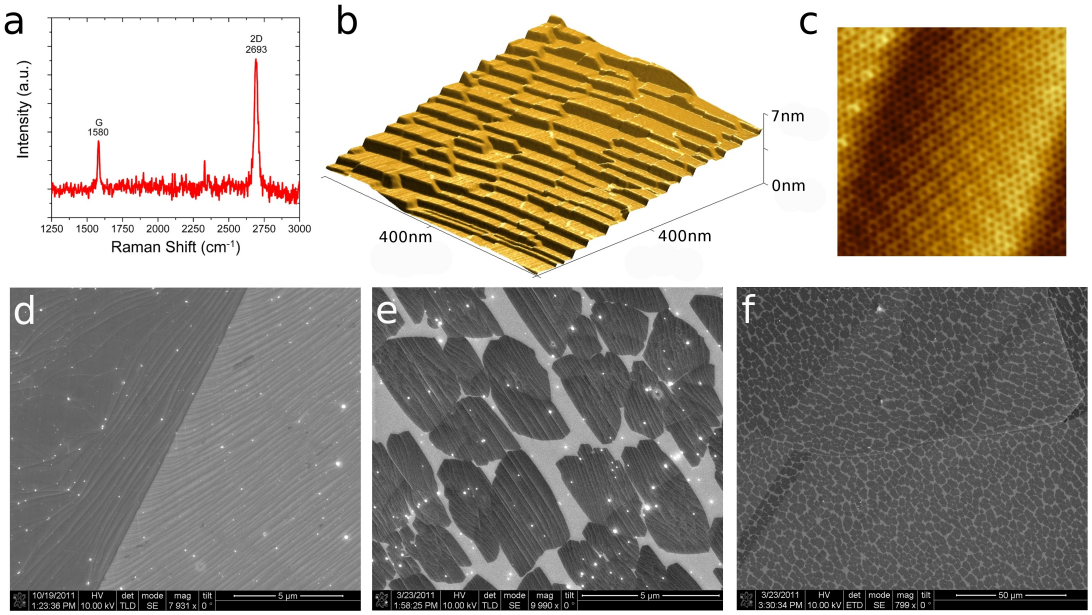

Supplementary Figure S1: Characterizing graphene growth on copper foils. a, Typical Raman spectrum of as grown graphene on copper after subtraction of copper luminescent background. The ratio of the two peaks (2D/G > 2) and line shape are consistent with monolayer growth. **b**, STM image of a large area of the copper surface covered with the graphene overlayer. **c**, Atomic resolution STM image of graphene continuously covering copper step edges. **d**, SEM image of a full graphene growth on a copper substrate. **e**, High magnification SEM image of a partial coverage growth of graphene on copper showing multiple individual islands nucleated on the surface, which ultimately lead to the continuous polycrystalline graphene studied. **f**, Low magnification SEM image of a partial coverage growth.

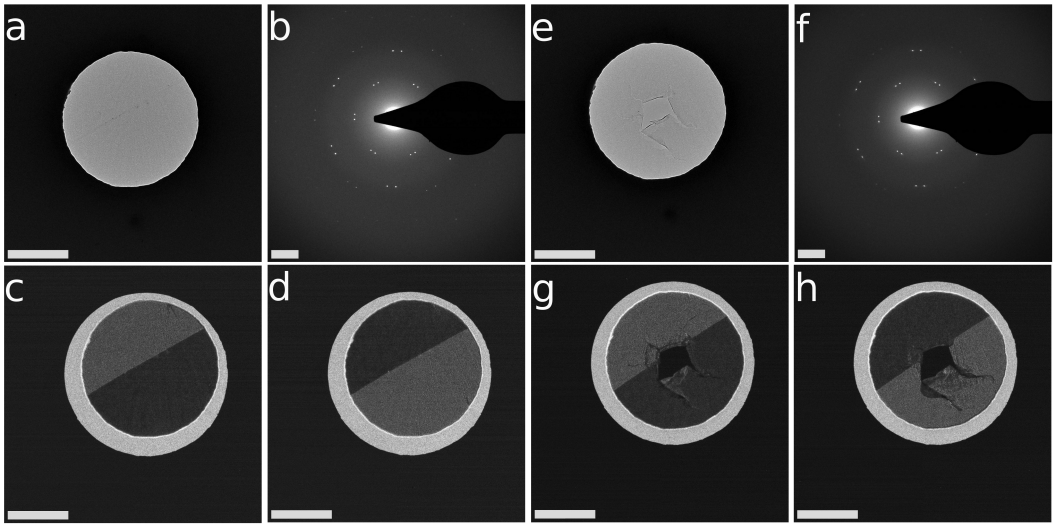

Supplementary Figure S2: Raw TEM data set of a bicrystal membrane. a and **b**, bright field TEM image and SAED pattern of a bicrystal graphene membrane before fracture measurements. **c** and **d**, two distinct dark field images acquired from the two diffraction patterns present in **b**. **e** and **f**, bright field TEM image and SAED pattern of the same membrane after fracture measurements. **g** and **h**, two distinct dark field images acquired from the diffraction patterns present in **f**. Scale bar in membrane images are 400 nm and in the SAED images are 4 nm^{-1}.

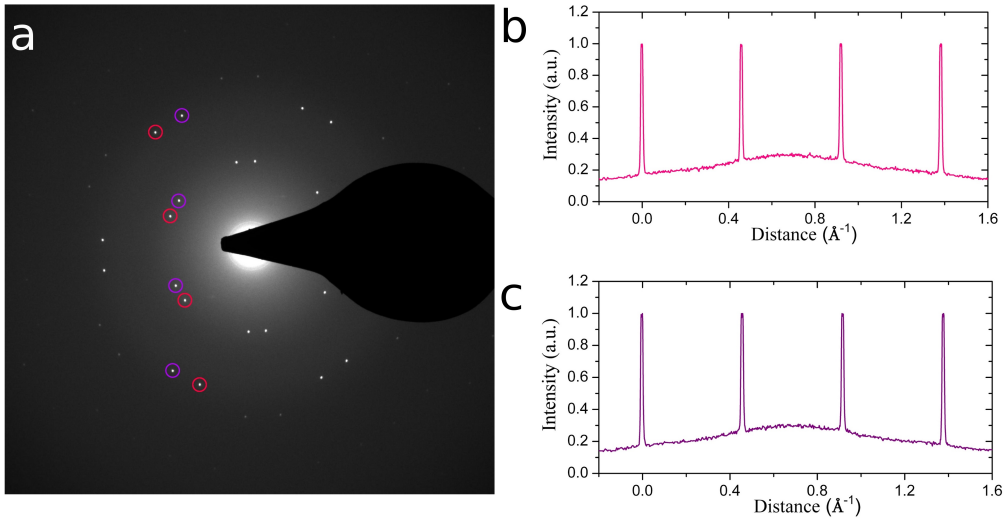

Supplementary Figure S3: Diffraction analysis. a, SAED pattern of a bicrystal membrane acquired at normal illumination incidence. **b**, Line profile taken along the four indicated spots in **a** belonging to one of the crystal regions. **c**, Line profile along the four spots in **a** belonging to the other crystal region. The ratio of the first and second order diffraction spots in both line profiles indicates stitching of monolayer crystal regions.

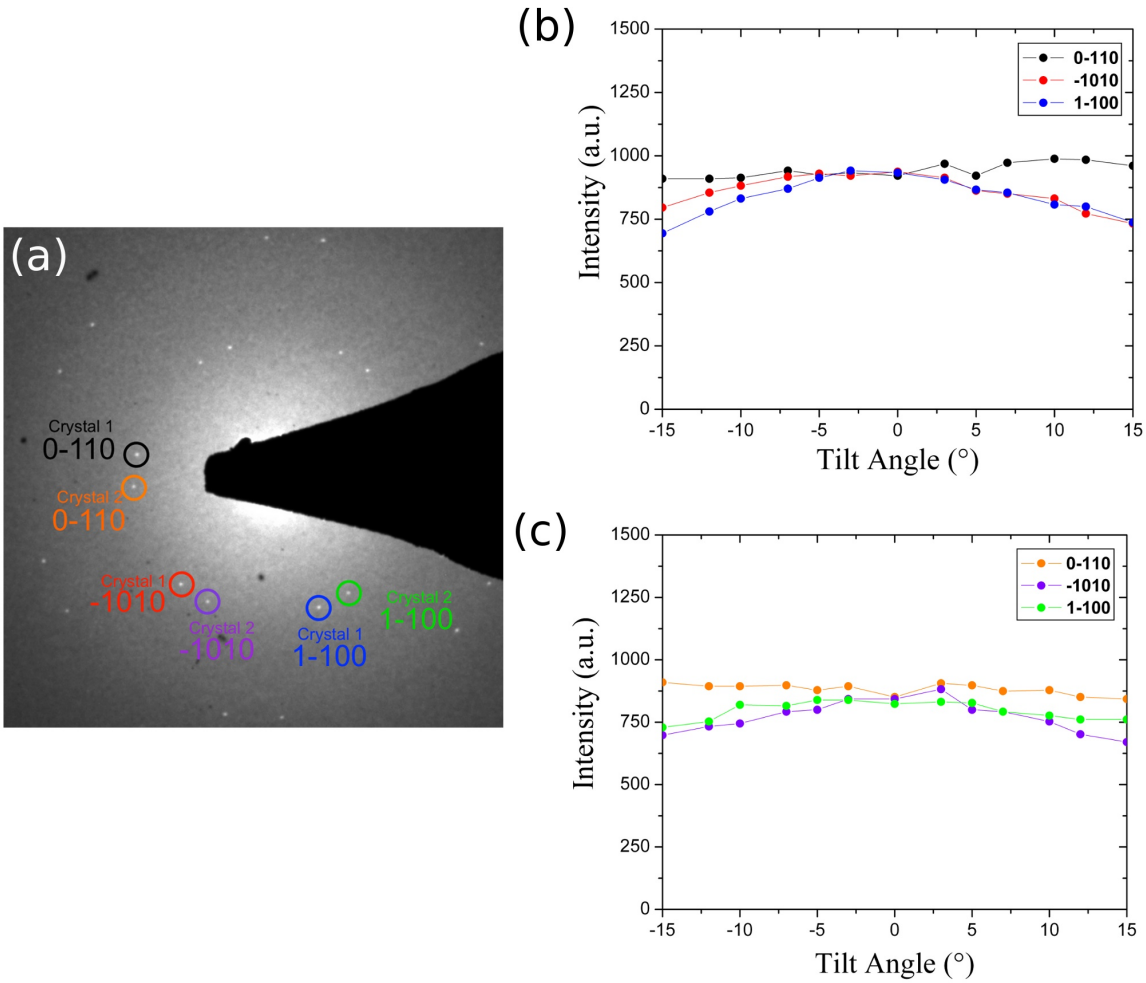

Supplementary Figure S4: Diffraction tilt analysis. a, SAED pattern of a bicrystal membrane acquired at normal incidence. **b**, Intensity as a function of tilt angle for the three diffraction spots of Crystal 1 of the bicrystal membrane. **c**, Intensity as a function of tilt angle for the three diffraction spots of Crystal 2 of the bicrystal membrane. The lack of significant intensity modulation as a function of tilt angle provides further confirmation of stitching of monolayer graphene crystal regions.

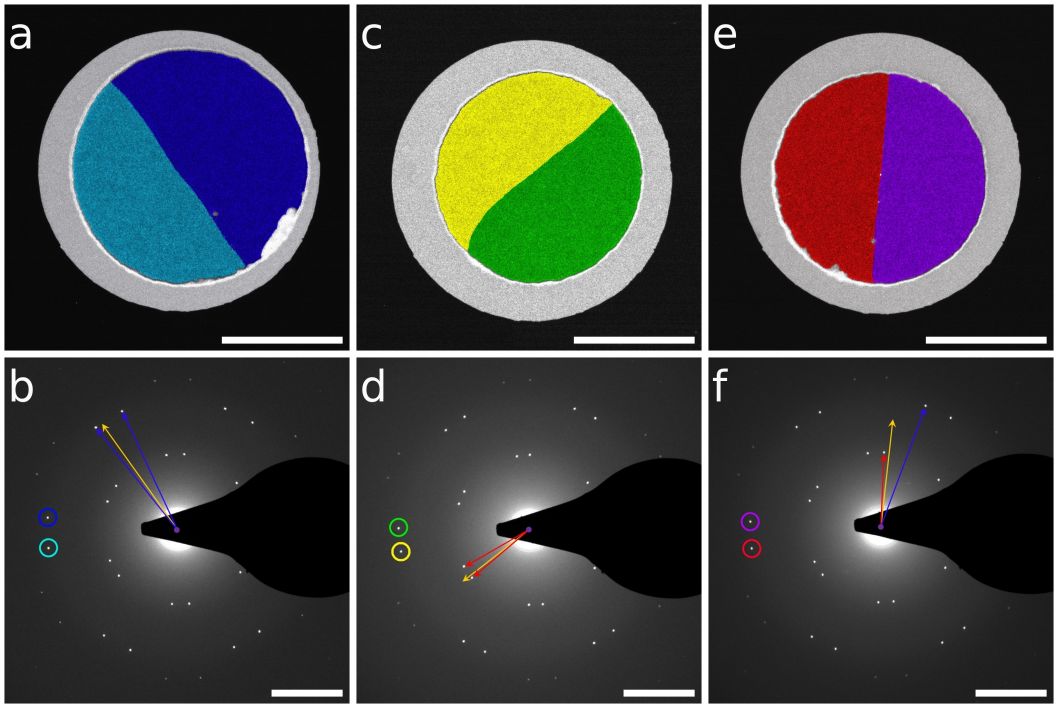

Supplementary Figure S5: Bicrystal membrane classification. a and **b**, Composite false color DF – TEM image of a ZZ bicrystal and its SAED pattern, respectively. Blue arrows correspond to the two distinct ZZ directions of each crystal region and the yellow arrow shows the direction of the grain boundary. **c** and **d**, Composite false color DF – TEM image of an AC bicrystal and its SAED pattern, respectively. Red arrows correspond to the two distinct AC directions of each crystal region and the yellow arrow shows the grain orientation. **e** and **f**, DF – TEM image of an AC – ZZ bicrystal and its SAED pattern, respectively. Red arrow indicates the AC direction of one grain and the blue arrow indicates the ZZ direction of the other grain. Yellow arrow shows the grain orientation. The colored circles in the SAED images show the aperture positions used for the DF images. Scale bars in **a**, **c**, and **e** are 500nm. Scale bars in **b**, **c**, and **d** are 5 nm^{-1}.

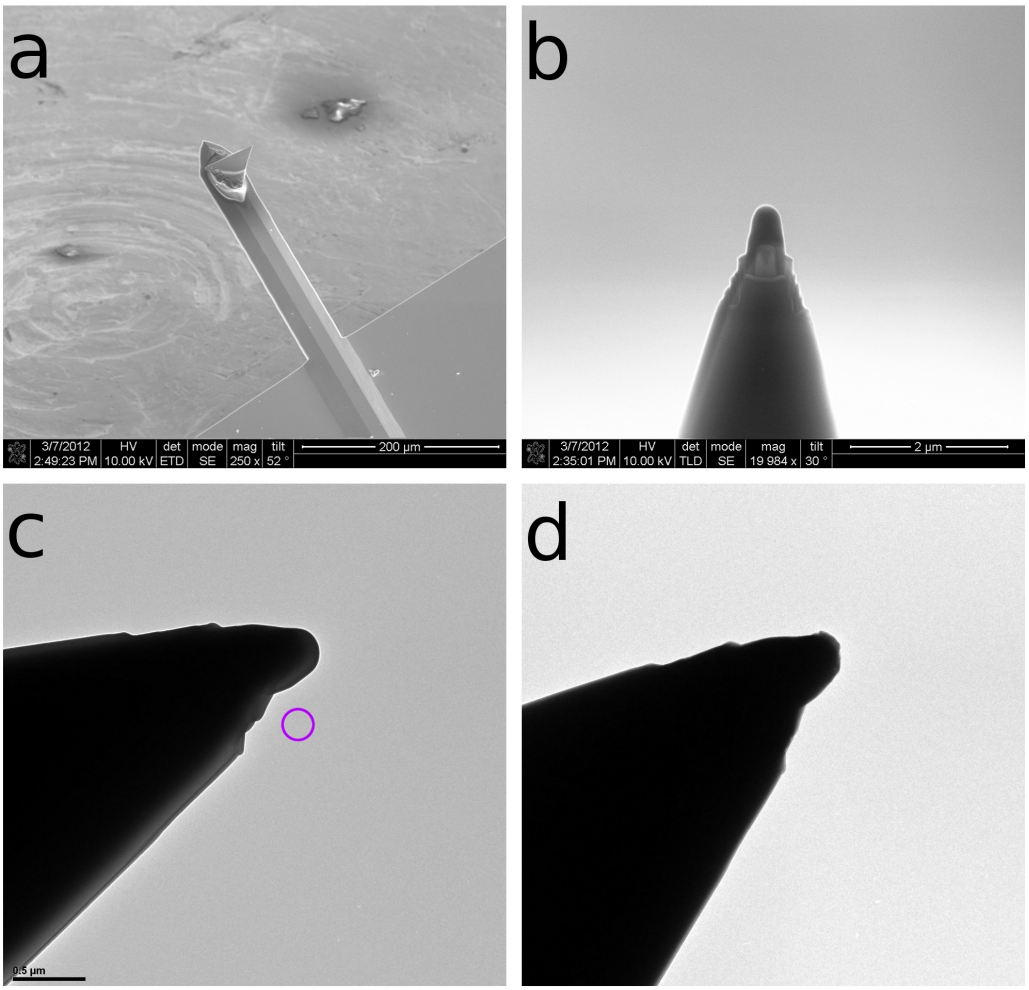

Supplementary Figure S6: Diamond tip characterization. a, Low magnification SEM image of the single crystal diamond tip used for fracture force measurements. A single crystal diamond wedge is mounted to a standard single crystal silicon cantilever. **b**, High magnification SEM image of the fabricated large radius single crystal diamond tip after FIB modification. **c**, Bright field TEM image of the diamond tip after FIB modification and before fracture force measurements. Purple circle follows the tip radius and has a diameter of 230 nm. **d**, Bright field TEM image of the diamond tip after fracture force measurements. The diamond tip structure and shape appear unaffected by the measurements, with the exception of a small accumulation of debris from the sample surface.

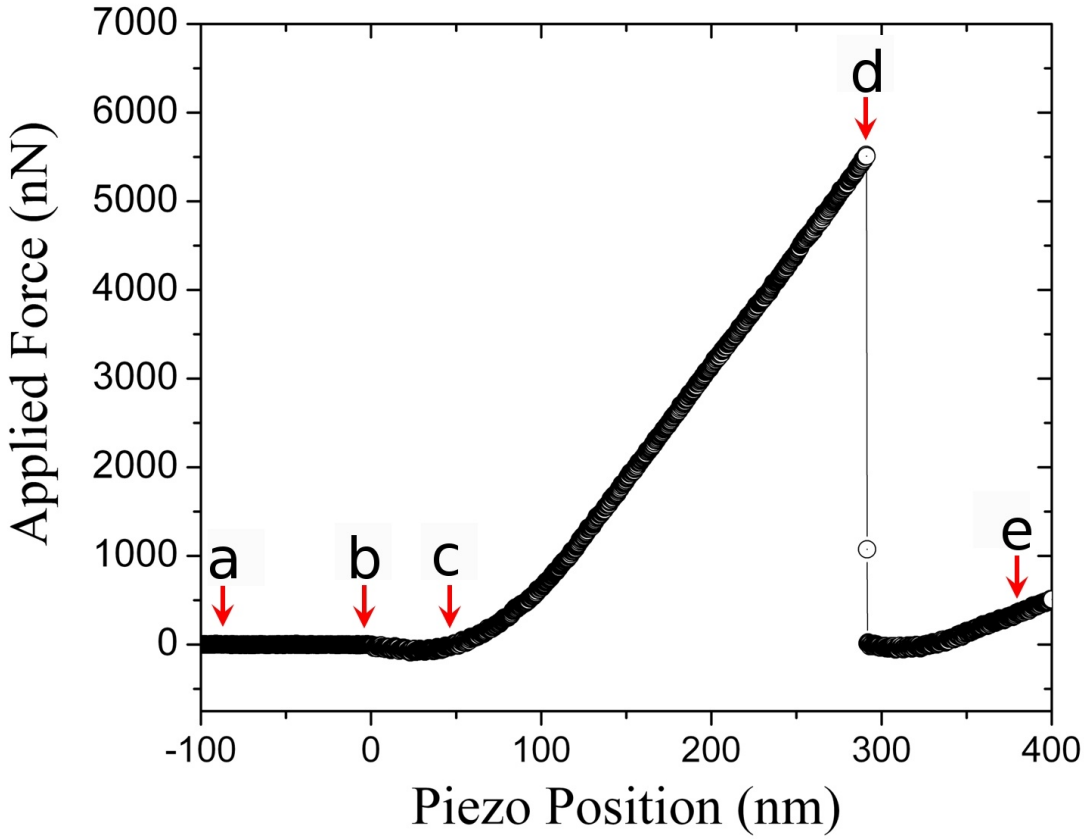

Supplementary Figure S7: Fracture force measurement. The cantilever is first approached to the surface of a membrane of interest. This is the region between points **a** and **b**. At the point of contact with the surface **b** the tip deflects down and snaps to contact due to the attractive Van der Waals force between tip and sample. Point **c** indicates an overall positive applied force to the graphene membrane and is continued to the point of fracture, **d**. The tip is pushed through the sample, **e** and then retracted to a safe distance above the sample. The region between **c** and **d** is the primary region of interest and is used for the force versus deflection plots given in Fig. 3. of the main text.

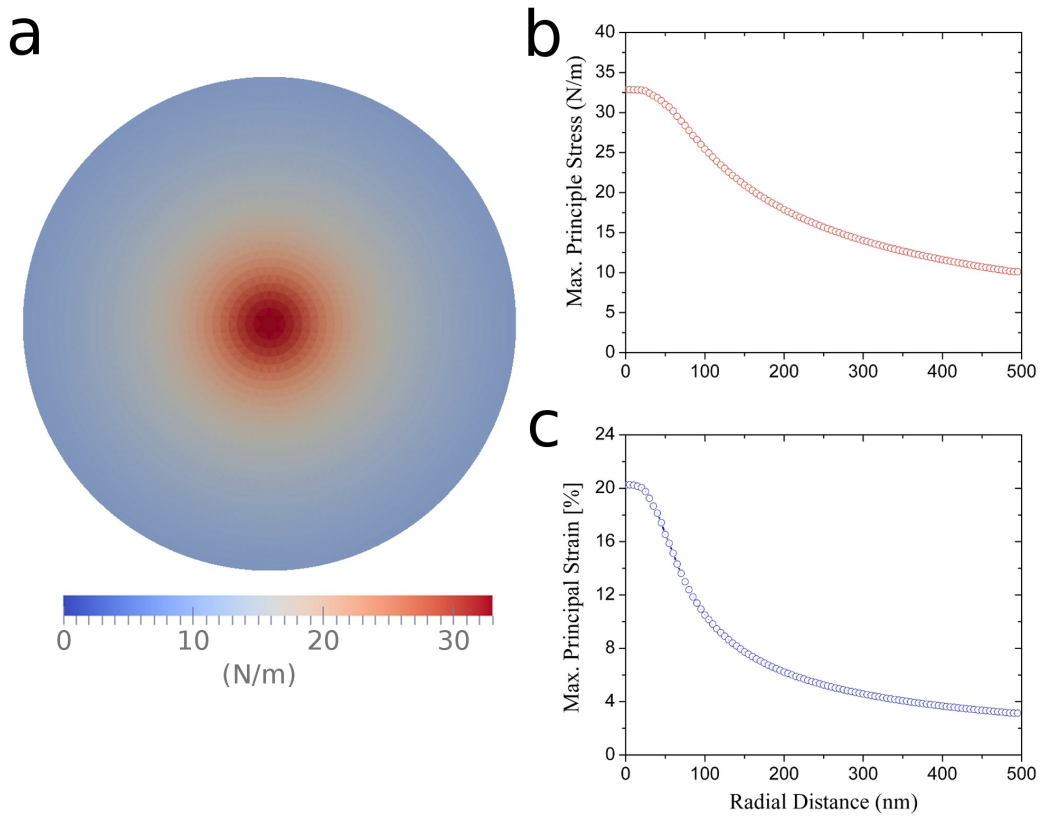

Supplementary Figure S8: FEA simulation of maximum principal stress and strain of a graphene membrane. a, The maximum principle stress distribution across a 1 micron graphene membrane indented with a 115 nm rigid spherical indenter at the point of rupture. **b**, Radial line profile of the maximum principle stress distribution along the ZZ direction of the graphene membrane. **c**, Radial line profile of the maximum principle strain distribution along the ZZ direction of the graphene membrane. By using a large tip indenter a significant portion of the membrane is near the maximum stress at fracture.

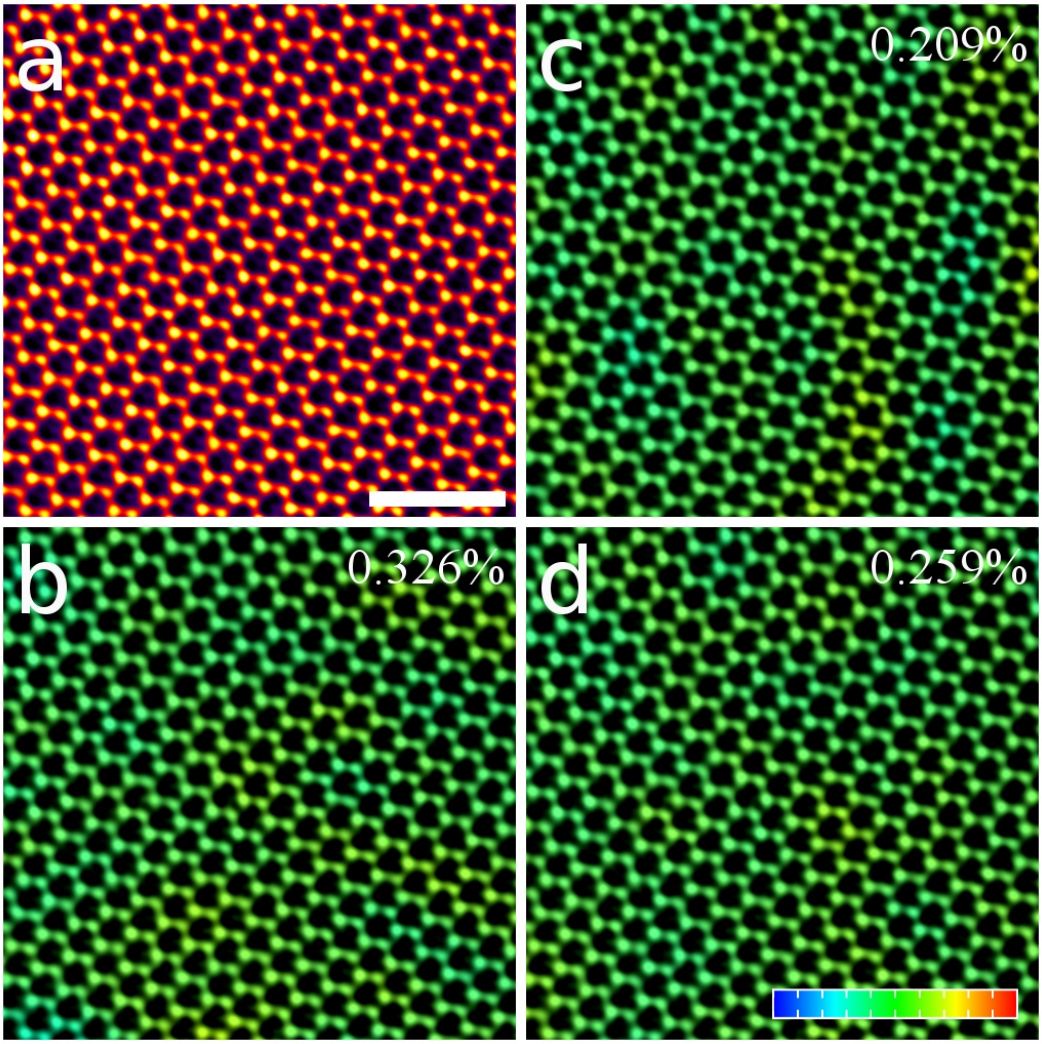

Supplementary Figure S9: Measured strain in single crystal graphene. a, AC-HRTEM image of a single crystal monolayer graphene region. **b**, Perpendicular strain field ($\boldsymbol{\varepsilon}_{yy}$) calculated from the single crystal image. **c**, Parallel field ($\boldsymbol{\varepsilon}_{xx}$) calculated from the image. **d**, Shear strain field ($\boldsymbol{\varepsilon}_{xy}$) calculated from the image. The standard deviation of the measured strain in the three strain fields are presented in the upper right corners of **b**, **c**, and **d**. The average strain values measured are 0% strain with a standard deviation of at most 0.326%. The color scale for the strain measurements can be found in **d**. The maximum and minimum strain color scale is -5% (blue) and +5% (red) in 1% increments. The scale bar can be found in **a** and is 1nm.

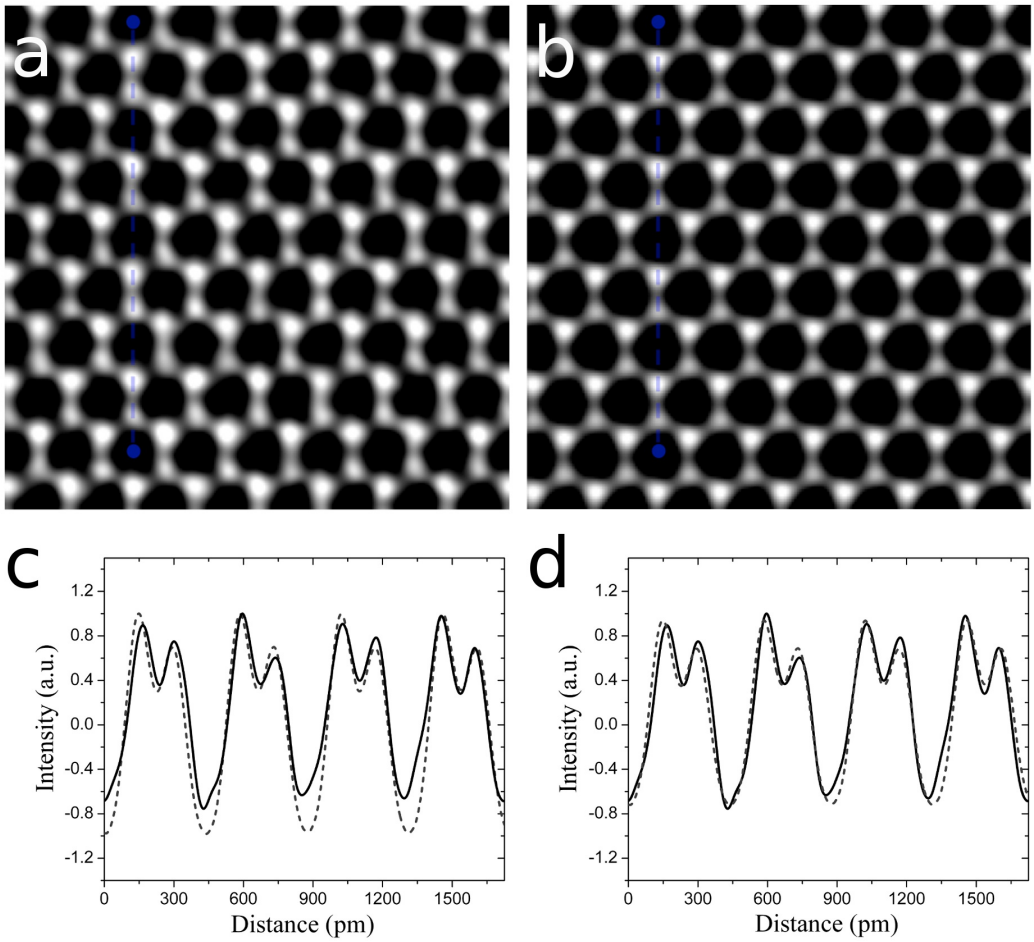

Supplementary Figure S10: Comparison of experimental and simulated AC-HRTEM images. **a**, Experimental AC-HRTEM image of a single crystal monolayer graphene region. The color scale in **a** has been shifted to highlight the peak positions of the individual carbon atoms. **b**, Multislice simulated AC-HRTEM image of a single crystal monolayer graphene region with the axial aberration known as three-fold astigmatism (A_2) having a value of 40nm at 60 degrees. The color scale in **b** has also been shifted to highlight the peak positions of the individual carbon atoms. **c**, Line profiles taken from the dashed lines of **a** and **b**. The solid black line corresponds to the experimental line profile taken from **a**. The dashed dark gray line corresponds to the simulated line profile taken from **b**. The lines have been normalized to their relative maximum peak intensity. This does not alter the relative contrast. **d**, The same line profiles from **c** are plotted against each other with the simulated line profile rescaled to match the maximum contrast of the experimental data.

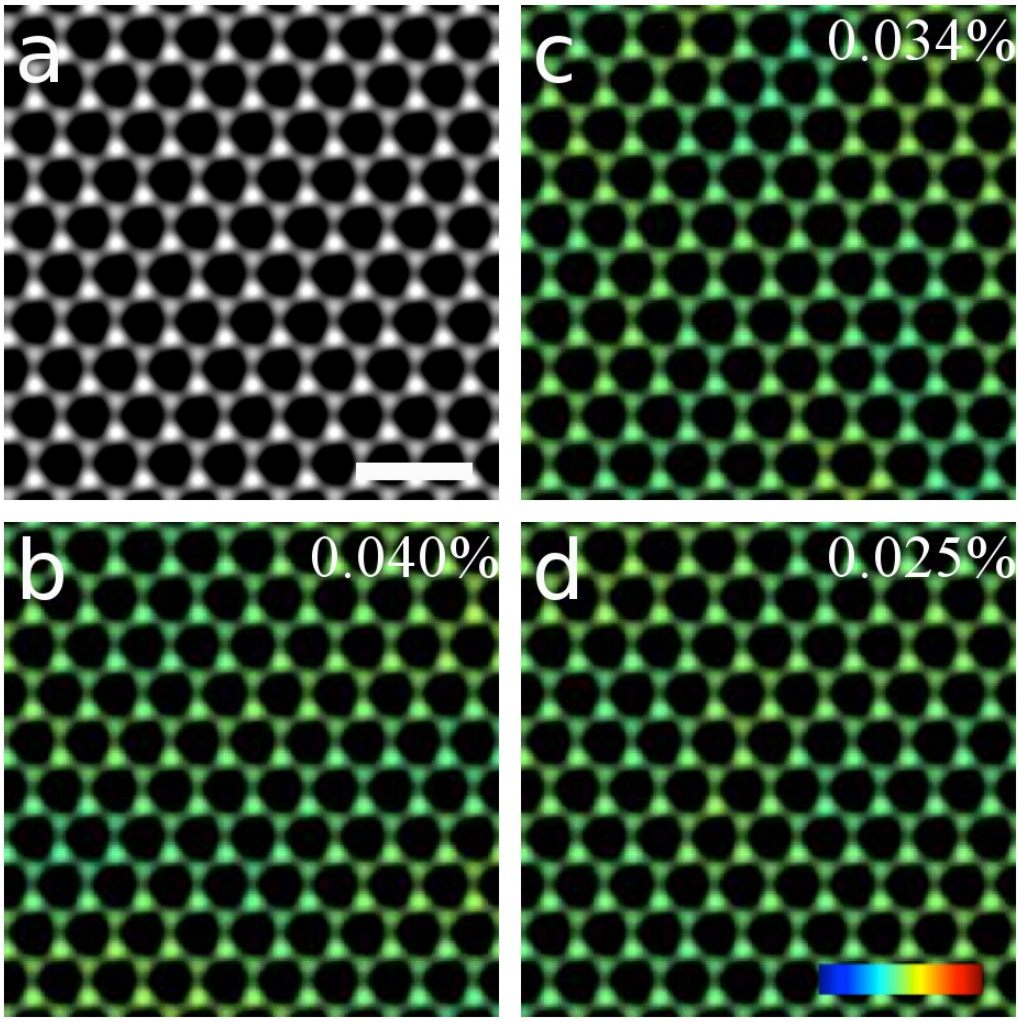

Supplementary Figure S11: Influence of three fold astigmatism (A_2) on strain analysis of simulated AC-HRTEM images. a, Simulated AC-HRTEM image of a single crystal monolayer graphene region. The color scale in **a** has been shifted to highlight the peak positions of the individual carbon atoms. **b**, Parallel strain field ($\boldsymbol{\varepsilon}_{xx}$) calculated from the simulated image. **c**, Perpendicular strain field ($\boldsymbol{\varepsilon}_{yy}$) calculated from the simulated image. **d**, Shear strain field ($\boldsymbol{\varepsilon}_{xy}$) calculated from the simulated image. The standard deviation of the measured strain in the three strain fields are presented in the upper right corners of **b**, **c**, and **d**. The average strain values measured are 0% strain with a standard deviation of at most 0.04%. This is approximately 100 times smaller than the measured strain values for the experimental data. The color scale for the strain measurements can be found in **d**. The maximum and minimum strain color scale is +/- 1% strain. This is five times smaller than the scale shown for the experimental strain values measured on the graphene grain boundary.

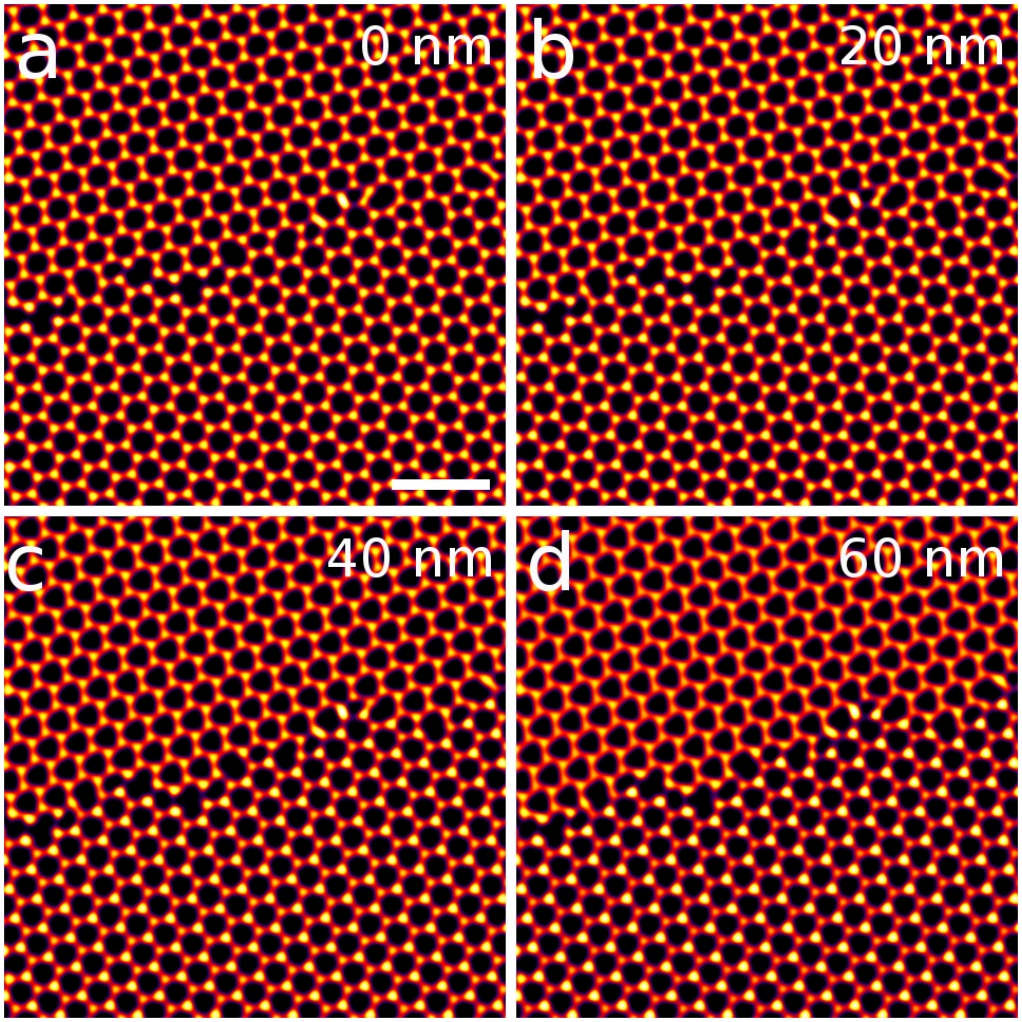

Supplementary Figure S12. Simulated graphene grain boundary image with varying A_2. a – d, Simulated images of the graphene grain boundary presented in the manuscript with 0 – 60 nm of A_2 at 110 degree orientation. The value of A_2 for each image is presented in the upper right corner of each panel. The scale bar is 0.8nm. The distortion by the three fold astigmatism, A_2, of the upper lattice is noticeably different than the lower lattice, which is the result of the symmetry of the aberration and the orientations of the two lattices with respect to the aberration direction.

Supplementary Methods

Graphene Synthesis

Graphene is grown on copper foil in a quartz tube furnace. Copper foil (Alfa Aesar, 25 μm thick, 99.999% purity) is loaded into a 2 inch quartz tube and heated under a H_2 flow (5 sccm) at a pressure of 250 mTorr and temperature of 1035 °C for 1.5 hours. For graphene growth, methane is introduced into the furnace and flowed (35 sccm) for 15 minutes with a growth pressure of 500 mTorr. This produces full graphene coverage over the entire copper surface. Upon completion, the furnace is cooled to room temperature under a constant CH_4 and H_2 flow (5:35 sccm) at the set pressure of 500 mTorr. Grown graphene on copper is characterized with Raman spectroscopy, scanning tunneling microscopy (STM), and scanning electron microscopy (SEM) before fabricating samples for force measurements. Raman spectroscopy is acquired using a Renishaw Micro Raman microscope with a 514 nm laser. STM images are acquired using a homebuilt STM. SEM images were acquired using a FEI Nova 600 Dualbeam SEM/FIB. Supplementary Figure S1 illustrates the general characterization of as-grown graphene on copper substrates.

Graphene Membrane Preparation

The graphene membranes are fabricated by transferring graphene from full coverage growth on copper substrates to a receiving TEM chip. Upon confirmation of graphene synthesis, a spin coating of 1% poly(methyl methacrylate) (PMMA) by weight in anisole is applied to the substrate at a spin speed of 4000 rpm for 45 seconds. The copper is etched using a commercial etchant (Transene, CE-100). The resulting PMMA supported graphene is rinsed in a deionized water and aqueous HCl bath, prior to a final deionized water rinse. The rinsed film is then applied to the receiving TEM substrate (Electron Microscopy Science, Dura SiN). In order to obtain clean suspended graphene membranes, the PMMA is removed by baking the sample in a H_2 – Ar gas mixture at a vacuum pressure of 7.5 Torr and temperature of 325 °C for one hour.

Low Voltage TEM Imaging

All TEM work done to structurally characterize samples for mechanical strength testing is performed at a low operating voltage of 60 kV in an FEI Technai T12 TEM. Dark – field TEM images were acquired with exposures between 10 and 20 seconds. Each diffraction spot of two distinct graphene grains of each bicrystal were imaged with the dark field mode to ensure that the

membranes were comprised of two distinct regions and not a rotated bilayer covering a single layer region. A complete TEM data set is presented in Supplementary Figure S2. In addition, the SAED patterns reveal that each bicrystal graphene membrane is comprised of two fused monolayer regions by analyzing the diffraction spot intensities. A typical SAED pattern acquired at normal incidence and line profile analysis, revealing stitching of two monolayer graphene crystal regions is presented in Supplementary Figure S3. Further confirmation of the monolayer stitching across grain boundaries is provided in the tilt series[46,47] data presented in Supplementary Figure S4. For angle determination and grain boundary classification of different bicrystals, a series of false colored DF-TEM images and the corresponding bicrystal membrane diffraction patterns are provided in Supplementary Figure S5.

Large Radius Single Crystal Diamond AFM Tip Fabrication

A commercially available sharp single crystal diamond tip (Micro Star Technologies) with a nominal radius of 20 nm was shaped in a FEI Nova 600 dual beam scanning electron microscope (SEM) – focused ion beam (FIB). The initial tip was first removed with the FIB and a large radius tip was then shaped using a defocused beam for a smooth tip radius. All the FIB work was performed at an operating voltage of 30 kV and a current set point of 10 pA. Once fabrication was complete, the tip shape was characterized with the SEM and TEM. After all the fracture force measurements were complete, the tip was again characterized with the SEM and TEM to ensure that the diamond indenter remained completely intact. Upon close inspection of the diamond tip it was clear that the tip shape and structure did not change, but only picked up a small amount of electron transparent debris from the fracture measurements. SEM and TEM images of the diamond tip characterization are presented in Supplementary Figure S6.

Fracture Force Determination in an AFM

Fracture measurements were performed in a Bruker AXS Dimension Icon AFM with a closed loop scan head. The spring constant calibration of the cantilever was accomplished by approaching the diamond tip onto a reference cantilever with a known spring constant near the expected spring constant of the measurement lever. Then a series of force spectroscopy measurements were performed. After calibration, the tip was used to image the membrane of interest to find the position of indentation. The tip was allowed to load and unload the surface

with small displacements to ensure no hysteresis in the measurement. Lastly, the tip was allowed to press into the membranes at a loading rate of 1 Hz over a piezo sweep distance of 600 nm. The subsequent graphene membrane deflection is obtained by subtracting the tip deflection measured at the photo diode from the *z*-piezo displacement. A plot of the raw data after conversion of the voltage at the photo diode into an applied force is presented in Supplementary Figure S7, which also describes the different points in a typical force measurement data set.

Finite Element Analysis of Graphene Fracture Strength

The indentation of graphene is simulated with a finite element implementation of nonlinear membrane elasticity based on finite-deformation (large-strain) kinematics. The stress-strain response of graphene is modeled by the 5th order anisotropic strain energy of Wei, *et. al.*(Ref. 36 of the main text). Meshes of 10981 nodes and 5400 quadratic triangular elements with C^0-Lagrange interpolation are used for the simulated membrane. Contact between the membrane and a rigid indenter was modeled as frictionless, and enforced with a standard Augmented-Lagrange constraint implementation. Fixed displacement boundary conditions are imposed along the circular boundary, and indentation forces are applied via displacement control. The nonlinear finite-element equilibrium equations are solved by the iterative Quasi-Newton L-BFGS-B method. The membrane failure (ultimate force at fracture) is estimated by the state in which the nonlinear solver diverged. The maximum principle stress and strain distribution in the membrane at failure is shown in Supplementary Figure S8.

Aberration Corrected High Resolution Transmission Electron Microscopy (AC-HRTEM) of Graphene

All AC-HRTEM images of graphene were acquired using TEAM 0.5 at the National Center for Electron Microscopy (NCEM) in Lawrence Berkeley National Laboratory (LBNL). The microscope is a modified FEI Titan microscope with a high brightness Schottky-field emission gun, monochromator, and spherical aberration corrector. The microscope is operated at 80 kV with the monochromator turned on to provide an energy spread of approximately 0.11eV. Images were acquired with exposures of 4 seconds, which provided high signal-to-noise and minimal image blur due to sample drift.

Realspace Strain Measurements in Graphene Grain Boundaries

We determine the initial atomic positions from intensity peaks in the micrograph. The peak positions are refined by fitting 2D Gaussian functions to each position simultaneously. Best-fit lattices for each grain are computed using linear regression. At the grain boundary, each atomic position is assigned to the grain that had the closest ideal lattice position. For each atomic position, displacement vectors are defined as the deviation from the ideal lattice positions. These measurements are resampled into continuous 2D displacement maps using Gaussian kernel density estimation with a bandwidth equal to the unit cell length. Lastly, the perpendicular ($\boldsymbol{\varepsilon_{yy}}$), parallel ($\boldsymbol{\varepsilon_{xx}}$), and shear ($\boldsymbol{\varepsilon_{xy}}$), strain maps are calculated by numerical differentiation of the displacement maps. The parallel direction (x-direction) of the grain boundary in Figure 4 was set to the crystallographic orientation closest to the grain boundary. The grain boundary is tilted approximately 3 degrees from the x-direction, and the grain boundary has a perfect 30 degree misorientation within the accuracy of the AC-HRTEM measurement.

Multislice Simulation for AC-HRTEM Strain Analysis

The simulated HRTEM micrographs of an ideal graphene lattice were generated with the multislice method and potentials given by E. J. Kirkland[48]. This method was implemented using custom MATLAB code. The frozen phonon approximation was used to account for thermal vibration. The 80 kV electron wave was assumed to be quasicoherent with a convergence angle of 150 µrad and a defocus spread of 1.5 nm. The radially symmetric wave aberrations included were C_1 = 4.5 nm, C_3 = -10 µm and C_5 = 4 mm. The carbon-carbon bond intensity asymmetry is attributed to three-fold astigmatism A_2 and this aberration was simulated up to a magnitude of 80 nm over a range of directions. The A_2 value of 40nm at a direction of 60 degrees appears to match the experimental images. The comparison between experimental and simulated images are presented in Supplementary Figure S10. A value of 40nm of A_2 at 60 degrees does not have a significant affect on the measured strain. This analysis is presented in Supplementary Figure S11.

Supplementary References

46. Meyer, J. C. *et al.* The structure of suspended graphene sheets. *Nature* **446**, 60 (2007).

47. Meyer, J. C. *et al.* On the roughness of single- and bi-layer graphene membranes. *Solid State Commun.* **143**, 101 (2007).

48. Kirkland, E. J. *Advanced Computing In Electron Microscopy*. (Springer, New York, 2nd Edition, 2010)